Nanoscale mapping of temperature and defect evolution inside operating AlGaN/GaN high electron mobility transistors

Chung-Han Lin,[1,a)] T. A. Merz,[2] D. R. Doutt,[2] M. J. Hetzer,[2] Jungwoo Joh,[3] Jesús A. del Alamo,[3] U. K. Mishra,[4] and L. J. Brillson[1,2,5]

[1]*Department of Electrical and Computer Engineering, The Ohio State University, Columbus, Ohio 43210, USA*
[2]*Department of Physics, The Ohio State University, Columbus, Ohio 43210, USA*
[3]*Microsystems Technology Laboratories, MIT, Cambridge, Massachusetts 02139, USA*
[4]*Department of Electrical and Computer Engineering and Department of Materials, UC-Santa Barbara, California 93106, USA*
[5]*Center for Materials Research, The Ohio State University, Columbus, Ohio 43210, USA*

We used depth-resolved microcathodoluminescence spectroscopy (DRCLS) and Kelvin probe force microscopy (KPFM) to measure and map the temperature distribution and defect generation inside state-of-the-art AlGaN/GaN-based high electron mobility transistors (HEMTs) on a scale of tens of nanometers during device operation. DRCLS measurements of near band edge energies across the HEMT's source-gate-drain regions reveal monotonic temperature increases across the submicron gate-drain channel, peaking under the drain side of the gate. DRCLS defect emissions mapped laterally and localized depthwise near the two-dimensional electron gas interface increase with device operation under the drain-side gate and correlate with higher KPFM surface potential maps. © 2009 American Institute of Physics. [DOI: 10.1063/1.3189102]

GaN-based high electron mobility transistors (HEMTs) have gained considerable importance as high power, high frequency devices.[1–4] However, high current density in the channel region leads to significant Joule heating that degrades device performance by decreasing carrier mobility,[5–9] thermal conductivity, and thermodynamic stability. Nanoscale-resolved measurements of temperature, defects, and electronic properties inside operating HEMT structures can reveal physical mechanisms of degradation under realistic conditions. Here we use a combination of laterally and depth-resolved microcathodoluminescence spectroscopy (DRCLS) (Ref. 10) with atomic force microscopy (AFM) and Kelvin force probe microscopy (KPFM) to monitor temperature, defect energies and densities, and electric potential across source-gate-drain channels of state-of-the-art AlGaN/GaN HEMTs grown on both sapphire and SiC. Temperature and defect emission maps are localized laterally and depthwise on a scale of tens of nanometers near the two-dimensional electron gas (2DEG) interface.

AlGaN/GaN device temperatures have been measured previously by visible or ultraviolet micro-Raman methods[11–16] and scanning thermal microscopy.[17] Both experimental[11,12,14–16] and simulation[6,12,15,16] results show that hot spots and dislocations form near the gate on the drain side. Semiconductor dislocations[18] and defect states[19] may degrade mobility, heat distribution, and device characteristics. Accurate spatially localized temperature and materials measurements are important for device modeling and failure analysis. However, submicron lateral and nanoscale layer HEMT features can present challenges in some cases due to diffraction and extended absorption depths, respectively.

We present results for two sets of AlGaN/GaN HEMTs, termed U-08 and M-01. U-08 heterostructures grown by metal-organic chemical vapor deposition consist of unintentionally doped (UID) GaN on a sapphire substrate followed by a 0.7 nm AlN interfacial layer, 40 nm layer of $Al_{0.22}Ga_{0.78}N$, 10 nm silicon-doped (7×10^{18} cm^{-3}) graded ($0 \leq x \leq 0.22$) $Al_xGa_{1-x}N$, and a 250 nm UID GaN cap. The UID GaN cap layer is etched away to form source, drain, gate contact, and an "extrinsic drain-source" region, defined as those regions between gate and drain and between gate and source. M-01 consists of nominally the same layer sequence but grown on SiC with a 640 nm Si_3N_4 passivation layer versus the UID GaN cap.

A JEOL JAMP-7800F ultrahigh vacuum (UHV) scanning electron microscope (SEM) with nm-scale resolution excited electron-hole pair recombination and cathodoluminescence (CL) with electron beam energies E_B ranging from 5 to 20 keV. We used layer-dependent Monte Carlo simulations[20] to select E_B that probe near the AlGaN/GaN 2DEG heterointerface. An Oxford MonoCL grating monochromator and Hamamatsu photomultiplier tube collected optical emission signals from samples at low ($\sim$12 K) and room temperature. A Park XE-70 AFM/KPFM provided simultaneous topography and potential maps.[21] An Agilent 4145B analyzer enabled electrical stress measurements.

Figure 1 shows the U-08 temperature distribution between gate and drain, termed the "extrinsic drain region," with beam current $I_B \sim 0.5$ nA. Peak electron-hole pair excitation depth U_0 derived from Monte Carlo simulation is $\sim$125 nm for $E_B = 5$ keV, just 75 nm below the 2DEG channel region. DRCLS provides local temperatures since the GaN near band edge (NBE) emission energy varies as $E_g(T) = E_g(0) - (5.98 + 0.12 \times 10^{-4}$ eV/C$)T$ for temperature T and band gap E_g.[22] Under low power (source-drain voltage $V_{DS} = 3.5$ V, gate-source voltage $V_{GS} = -2$ V, and drain-
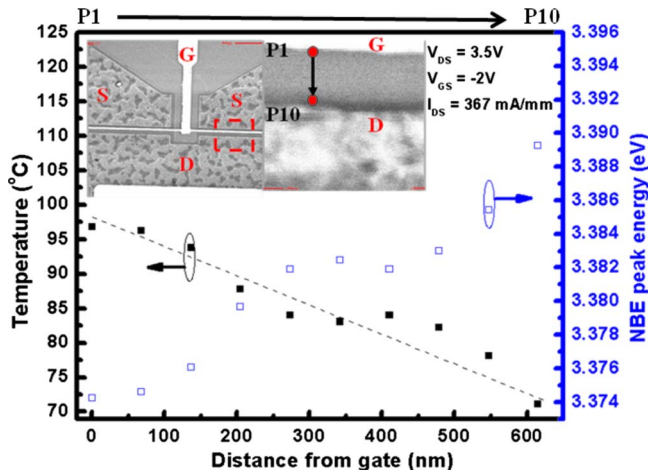
a)Electronic mail: chunghan.lin@gmail.com.

FIG. 1. (Color online) Temperature distribution of U-08 operated at V_{DS} =3.5 V and V_{GS}=−2 V. P1 is nearest the gate while P10 is furthest away. Inset photograph shows SEM image of source-drain region measured.

source current I_{DS}=367 mA/mm), Fig. 1 shows temperature increasing from drain to gate along ten equally spaced points along a perpendicular to and between gate and drain, consistent with micro-Raman results[11–14] and other techniques but with dramatically higher spatial and depth resolution. Localized electron beam heating produces no measurable NBE temperature rise at room temperature. At I_B=0.5 nA and E_B=5 keV, induced beam currents are ~0.2 μA, negligible compared to our device currents. Piezoelectric strain can shift NBE energies by 24 meV/GPa (Ref. 23) =40 °C/GPa, but V_{SD}=40 V produces strains of ~0.4 GPa at the drain[24] that extrapolate linearly to <1 °C for V_{SD}=6 V here.

Figure 2(a) shows the SEM image of another U-08 GaN HEMT operated to failure (V_{DS}=3.5 V, V_{GS}=0 V, I_{DS} =633 mA/mm, 4 h) in UHV. AFM revealed a 100–150 nm deep, ~60 nm wide crater in the extrinsic drain region. A CL map of NBE (~3.42 eV at 12 K) emission in Fig. 2(b)
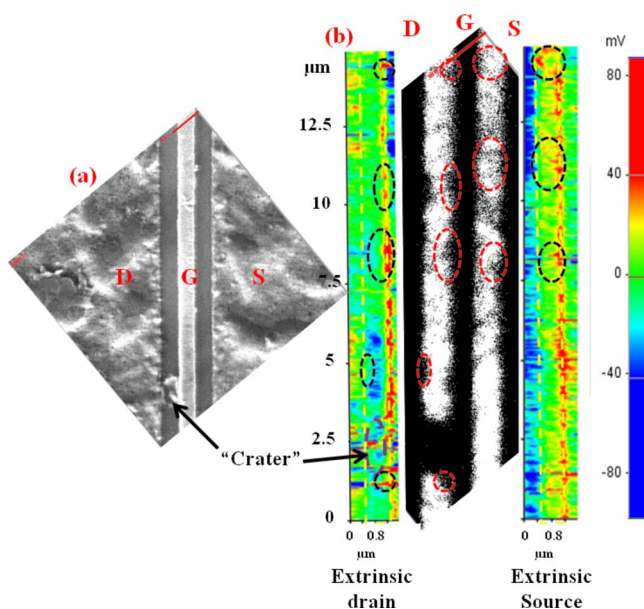

FIG. 2. (Color online) For U-08, (a) SEM image shows the Source (s), Gate (g), and Drain (d) region. (b) CL map of NBE emission (middle) and KPFM result (side) taken in the same (a) region. Red dashed circles show some of the same higher defect, higher potential region for CL and KPFM map, respectively, where devices degrade faster.
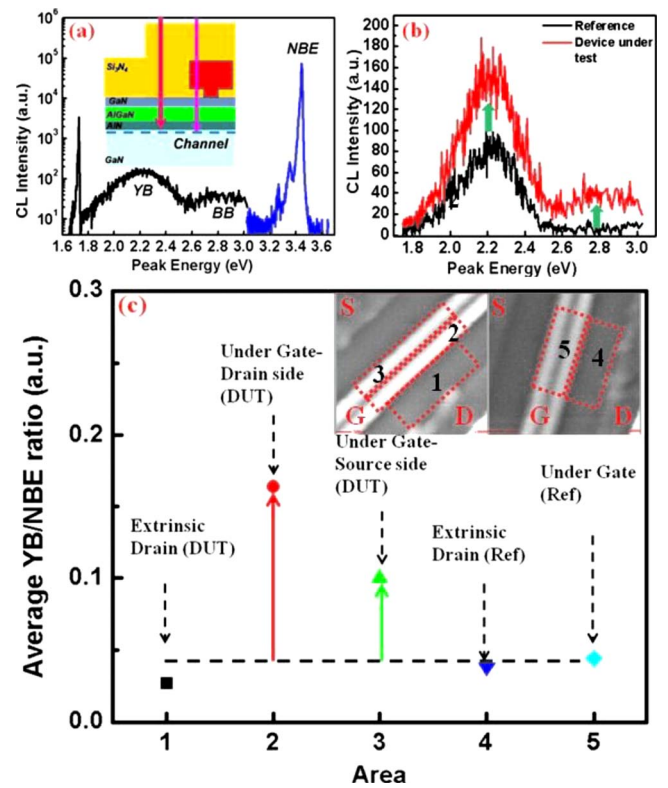

FIG. 3. (Color online) DRCLS results for M-01 sample, (a) DRCLS spectrum from under the gate overhang before operation; Inset: schematic of M-01 cross section. Arrow indicates incident electron beam path through gate overhang at E_B=20 keV. (b) increase in 2.2 eV YB emissions before [also (a)] and after 12 h, V_D=10 V, V_G=−2 V, 476 mA/mm operation. (c) Position-dependent average YB/NBE ratios showing largest increase under drain-side gate after 12 h operation. Inset shows SEM image and definition of areas 1–5.

shows (i) NBE disappearance at the failure region and (ii) variations in NBE intensity within the extrinsic drain and source. Bright CL map areas exhibit 1000-fold higher NBE intensity than dark areas in the extrinsic drain versus uniform intensity of the virgin sample. NBE intensity decreases apparent in Fig. 2(b) signify free carrier recombination at sub-band gap energies.

KPFM maps in Fig. 2(b) show nonuniform potential distribution. Dashed rectangles define the same extrinsic drain and source regions as in Fig. 2(a), while an ellipse outlines the "crater." Surface potentials vary by more than 100 meV within the unbiased extrinsic drain and source regions, with higher potentials in general corresponding to regions of reduced NBE emission (higher defect density). Surface photovoltage spectra (SPS) indicate defect levels 2.2 eV below the conduction band increasing in these regions.[25]

Varying E_B allowed us to preferentially excite not only unpassivated extrinsic drain and source regions but also regions passivated with dielectrics or shadowed by gate overhangs. Figure 3(a) shows a DRCL spectrum with features at $h\nu$=3.4 eV (NBE), 2.2 eV "yellow band" (YB), and 2.8–3.2 eV "blue band" (BB) (Ref. 26) taken from the drain-side gate overhang region for the virgin M-01 HEMT. YB emission is typically associated with Ga vacancies or Ga vacancy-impurity complexes in GaN.[23] The Fig. 3(a) inset illustrates the cross sectional HEMT passivation layer, gate and active layer geometry through which the electron beam can penetrate. For M-01, E_B=8 and 20 keV produce electron-hole

pairs peaking at ~660 and 1300 nm at the 2DEG layer next to versus through the gate overhang, respectively. Figure 3(b) illustrates the increase in YB defect emission after 12 h device operation (termed "Device under test") at $V_{DS}=10$ V, $V_{GS}=-2$ V, and $I_{DS}=476$ mA/mm (red curve) compared with emission (black) at the same location before operation ("Reference device").

Figure 3(c) displays the changes in YB to NBE defect emissions ratio versus position within the source-gate-drain region. Each data point representing the ratio $I(\text{YB})/I(\text{NBE})$ of defect versus NBE emission intensities corresponds to an average of spectra at the same distance from and along the width of the gate. Figure 3(c) shows that YB under the gate on the drain side increases by a factor of 3.5 compared with ~2.2x under the gate on the source side and very little within the extrinsic drain region. In contrast, averaged BB/NBE ratios shows no strong correlation with position. This result shows that device operation can increase defect emissions within AlGaN/GaN HEMTs. Figure 3(c) shows that the growth of such defect concentrations varies systematically across the source-drain-channel region. Furthermore, device operation affects defect changes preferentially. YB defect emission exhibits much larger and systematic increases than defects characterized by BB emission, indicating a link between this defect and device degradation. This 2.2 eV YB defect emission is attributed to transitions involving deep levels 2.2 eV below the conduction band,[26] consistent with SPS measurements for U-08.[25] Such defect formation during device operation could alter Fermi level positions, band bending, and hence potential within the surface layer. Consistent with a wealth of electrical stress studies,[27] these electrical and material changes may contribute to degradation of HEMT performance and ultimately device failure. After stressing, saturation current decreased 4%–6% and gate leakage current increased one order of magnitude, consistent with previous literature. Further details will be published elsewhere.

In summary, we have demonstrated the utility of electron microscope-based CL spectroscopy to probe temperature distributions on a nanometer scale inside state-of-the-art HEMTs during device operation. Consistent with previously published data, temperatures increase from drain to gate, reaching maximum values under the drain-side gate. Depth-resolved defect emission is distributed nonuniformly across the source-gate-drain region. Specific defect emissions related to Ga vacancies are found to increase with device operation, increasing from drain to gate, indicating that longer operation promotes increased YB defect formation. Overall, the nanoscale, depth-resolved optical, and scanned probe techniques reported here can be used to reveal and in principle predict physical mechanisms of AlGaN/GaN HEMT degradation under realistic conditions.

[1] Y. F. Wu, D. Kapolnek, J. P. Ibbetson, P. Parikh, B. P. Keller, and U. K. Mishra, IEEE Trans. Electron Devices **48**, 586 (2001).

[2] U. K. Mishra, P. Parikh, and Y.-F. Wu, Proc. IEEE **90**, 1022 (2002).

[3] O. Ambacher, B. Foutz, J. Smart, J. R. Shearly, N. G. Weimann, K. Chu, M. Murphy, A. J. Sierakowski, W. J. Schaff, L. F. Eastman, R. Dimitrov, A. Mitchell, and M. Stutzmann, J. Appl. Phys. **87**, 334 (2000).

[4] O. Ambacher, J. Smart, J. R. Shealy, N. G. Weimann, K. Chu, M. Murphy, W. J. Schaff, L. F. Eastman, R. Dimitrov, L. Wittmer, M. Stutzmann, W. Rieger, and J. Hilsenbeck, J. Appl. Phys. **85**, 3222 (1999).

[5] Y. Chang, Y. Zhang, Y. Zhang, and K. Y. Tong, J. Appl. Phys. **99**, 044501 (2006).

[6] W. D. Hu, X. S. Chen, Z. J. Quan, C. S. Xia, W. Lu, and P. D. Ye, J. Appl. Phys. **100**, 074501 (2006).

[7] S. A. Vitusevich, S. V. Danylyuk, N. Klein, M. V. Petrychuk, A. Yu. Avksentyev, V. N. Sokolov, V. A. Kochelap, A. E. Belyaev, V. Tilak, J. Smart, A. Vertiatchikh, and L. F. Eastman, Appl. Phys. Lett. **82**, 748 (2003).

[8] N. Braga, R. Mickevicius, R. Gaska, X. Hu, M. S. Shur, M. Asif Khan, G. Simin, and J. Yang, J. Appl. Phys. **95**, 6409 (2004).

[9] N. Braga, R. Mickevicius, R. Gaska, M. S. Shur, M. Asif Khan, and G. Simin, Appl. Phys. Lett. **85**, 4780 (2004).

[10] L. J. Brillson, J. Vac. Sci. Technol. B **19**, 1762 (2001).

[11] M. Kuball, J. M. Hayes, M. J. Uren, T. Martin, J. C. H. Birbeck, R. S. Balmer, and B. T. Hughes, IEEE Electron Device Lett. **23**, 7 (2002).

[12] M. Kuball, S. Rajasingam, A. Sarua, M. J. Uren, T. Martin, B. T. Hughes, K. P. Hilton, and R. S. Balmer, Appl. Phys. Lett. **82**, 124 (2003).

[13] J. W. Pomeroy, M. Kuball, D. J. Wallis, A. M. Keir, K. P. Hilton, R. S. Balmer, M. J. Uren, T. Martin, and P. J. Heard, Appl. Phys. Lett. **87**, 103508 (2005).

[14] J. W. Pomeroy, M. Kuball, M. J. Uren, K. P. Hilton, R. S. Balmer, and T. Martin, Appl. Phys. Lett. **88**, 023507 (2006).

[15] I. Ahmad, V. Kasisomayajula, M. Holtz, J. M. Berg, S. R. Kurtz, C. P. Tigges, A. A. Allerman, and A. G. Baca, Appl. Phys. Lett. **86**, 173503 (2005).

[16] I. Ahmad, V. Kasisomayajula, D. Y. Song, L. Tian, J. M. Berg, and M. Holtz, J. Appl. Phys. **100**, 113718 (2006).

[17] R. Aubry, J.-C. Jacquet, J. Weaver, O. Durand, P. Dobson, G. Mills, M.-A. di Forte-Poisson, S. Cassette, and S.-L. Delage, IEEE Trans. Electron Devices **54**, 385 (2007).

[18] J. Zou, D. Kotchetkov, A. A. Balandin, D. I. Florescu, and F. H. Pollak, J. Appl. Phys. **92**, 2534 (2002).

[19] W. Saito, M. Kuraguchi, Y. Takada, K. Tsuda, I. Omura, and T. Ogura, IEEE Trans. Electron Devices **52**, 159 (2005).

[20] http://www.gel.usherbrooke.ca/casino.

[21] D. R. Doutt, C. Zgrabik, H. L. Mosbacker, and L. J. Brillson, J. Vac. Sci. Technol. B **26**, 1477 (2008).

[22] A. P. Young and L. J. Brillson, Appl. Phys. Lett. **77**, 699 (2000).

[23] W. Rieger, T. Metzger, H. Angerer, R. Dimitrov, O. Ambacher, and M. Stutzmann, Appl. Phys. Lett. **68**, 970 (1996).

[24] A. Sarua, H. Ji, M. Kuball, M. J. Uren, T. Martin, K. J. Nash, K. P. Hilton, and R. S. Balmer, Appl. Phys. Lett. **88**, 103502 (2006); A. Sarua, T. Batten, H. Ji, M. J. Uren, T. Martin, and M. Kuball, CS Mantech Conference, May 2009 (unpublished).

[25] C.-H. Lin, T. A. Merz, D. R. Doutt, J. A. del Alamo, U. K. Mishra, and L. J. Brillson (unpublished).

[26] S. T. Bradley, A. P. Young, L. J. Brillson, M. J. Murphy, W. J. Schaff, and L. F. Eastman, IEEE Trans. Electron Devices **48**, 412 (2001).

[27] J. Joh and J. A. del Alamo, IEEE Electron Device Lett. **29**, 287 (2008), and references therein.